ELSEVIER

International Journal of Heat and Fluid Flow 21 (2000) 84–91

International Journal of HEAT AND FLUID FLOW

www.elsevier.com/locate/ijhff

The effect of extrusion slit on the flow and heat-transfer characteristics from a continuously moving material with suction or injection

Sami A. Al-Sanea, Mohamed E. Ali *

Department of Mechanical Engineering, King Saud University, P.O. Box 800, Riyadh 11421, Saudi Arabia

Received 1 December 1998; accepted 16 July 1999

Abstract

The flow and heat-transfer characteristics over a continuously moving horizontal material with suction or injection are studied very close and far away downstream from the extrusion slit. The finite-volume method is used to map out the solutions in the nonsimilar and similar regions subject to uniform surface velocity and temperature. The effects of Prandtl number (Pr), suction/injection parameter (d) and Reynolds number (Re_x) on the friction and heat-transfer coefficients are studied. Comparisons with the similarity method solutions downstream at high Re_x are made. Critical Reynolds numbers to distinguish between the self-similar and nonsimilar regions are obtained. The region very close to the slit is characterized by: (i) a rapid increase in skin-friction coefficient with increasing suction, or with increasing injection above $d \approx 0.45$; the lowest friction coefficient is attained at an injection parameter $d \approx 0.45$, and (ii) large heat-transfer coefficient which increases with increasing Prandtl number and suction, and decreases with increasing injection. On the other hand, downstream where the similarity solution is valid both the skin-friction and heat-transfer coefficients reach asymptotic values depending on d and, for the latter, on Pr.

Keywords: Stretched surface; Suction or injection; Finite volume; Nonsimilar region

Notation

$C_{f,x}$	local skin-friction coefficient, $\tau_{w,x}/0.5\rho u_w^2$
d	dimensionless suction/injection parameter, $v_w Re_x^{0.5}/u_w$
h_x	local heat-transfer coefficient
k	thermal conductivity
L	surface length
Nu_x	local Nusselt number, $h_x x/k$
p	pressure
P	dimensionless pressure, $(p-p_\infty)/\rho u_w^2$
Pr	Prandtl number
Re_x	local Reynolds number, $u_w x/v$
S	source term
T	temperature
u	velocity component in x-direction
U	dimensionless velocity component, u/u_w
v	velocity component in y-direction
V	dimensionless velocity component, v/u_w
x	coordinate along direction of surface motion
X	dimensionless coordinate, x/L
y	coordinate along direction normal to surface motion
Y	dimensionless coordinate, y/L

Greek

Γ	dimensionless diffusion coefficient
η	dimensionless similarity variable, $y(u_w/2vx)^{0.5}$
θ	dimensionless temperature, $(T-T_\infty)/(T_w-T_\infty)$
v	kinematic viscosity
ρ	density
$\tau_{w,x}$	local shear stress
ϕ	a general dependent variable

Subscripts

c	critical conditions
e	pertains to entrained velocity
w	condition at surface
ϕ	a general dependent variable
∞	condition at ambient medium
v	velocity boundary layer
T	thermal boundary layer

1. Introduction

A continuously moving surface through an otherwise quiescent medium has many applications in manufacturing pro-

* Corresponding author.

E-mail addresses: sanea@ksu.edu.sa (S.A. Al-Sanea), mali@ksu.edu.sa (M.E. Ali).

0142-727X/00/$ - see front matter
PII: S0142-727X(99)00062-4

cesses. Such processes are hot rolling, wire drawing, metal extrusion, crystal growing, continuous casting, glass fiber production, and paper production (Altan et al., 1979; Fisher, 1976; Tadmor and Klein, 1970). The study of flow field and heat transfer is necessary for determining the quality of the final products of such processes as explained by Karwe and Jaluria (1988, 1991).

Since the pioneer study of Sakiadis (1961) who developed a numerical solution for the boundary layer flow field of a stretched surface, many authors have attacked this problem to study the hydrodynamic and thermal boundary layers due to a moving surface. Tsou et al. (1967) reported, analytically and experimentally, the flow and heat-transfer fields developed by a continuously moving surface. Stretched surfaces with different velocity and temperature conditions at the surface were studied by Crane (1970), Soundalgekar and Murty (1980), Grubka and Bobba (1985) and Ali (1994).

Suction or injection through a stretched surface was introduced by Erickson et al. (1966) and Fox et al. (1968) for uniform surface velocity and temperature, and by Gupta and Gupta (1977) for a linearly varying surface velocity. Chen and Char (1988) have studied the suction or injection on a linearly varying plate velocity subject to uniform wall temperature and heat flux; the more general case using a power law velocity and temperature distribution at the surface was studied by Ali (1995). Laminar mixed convection, from a uniformly moving vertical surface, was considered with suction or injection for uniform and variable surface temperature by Ali and Al-Yousef (1997, 1998), respectively. In their study, solution domains have been obtained when the buoyancy force assisted or opposed the induced flow for different Prandtl numbers.

In almost all the papers cited earlier, the studies concentrated on the boundary layer far away from the extrusion slit where the boundary layer approximations and, hence, the similarity method are valid. However, in most practical applications, the flow and heat-transfer characteristics are very important close to the slit at which both the friction and heat-transfer coefficients attain their largest values. On the other hand, the finite-difference method using the full governing equations was used by Karwe and Jaluria (1988, 1991), for uniformly moving flat plate with a uniform temperature at the slit, to study the effects near the slit from which the plate emerges. Furthermore, Kang and Jaluria (1993) included the buoyancy effects on moving plate in materials processing. In these papers, the suction or injection at the moving plate was relaxed. However, during the manufacture of some materials such as plastic and rubber sheets it is often necessary to blow a cooling gaseous medium through the not-yet-solidified material (Lakshmisha et al., 1988). The present study focuses on the effect of suction and injection at the moving surface using the full governing equations. Special attention is given to the region very close to the slit, and to obtain critical Reynolds numbers that distinguish the similar from the nonsimilar regions for both the velocity and thermal boundary layers. Comparison with the similarity method solution is made far downstream.

The mathematical formulation of the problem is presented in Section 2, followed by the numerical solution procedure in Section 3. In Section 4 results and discussion are reported and finally conclusions are given in Section 5.

2. Mathematical formulation

2.1. Basic assumptions and governing equations

Fig. 1 shows a continuously moving plate emerges from a slit at a velocity u_w and a temperature T_w in an otherwise quiescent medium with suction or injection at the plate. The induced motion of the fluid is assumed to be laminar, steady, and two dimensional with thermal active incompressible viscous fluid with constant properties. Subject to these assumptions the governing equations in dimensionless form can be written as:

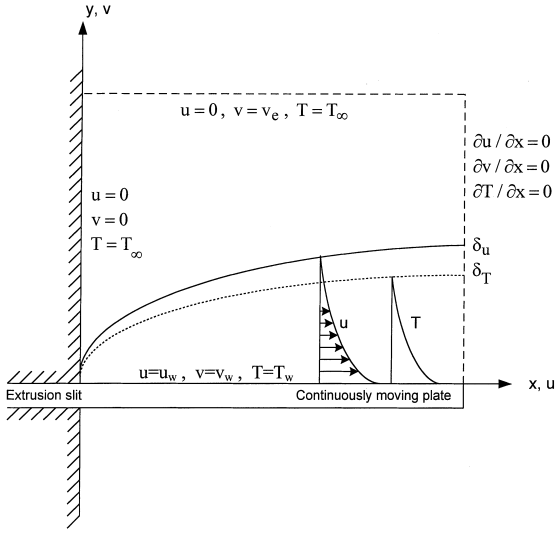

Fig. 1. A schematic showing the physical situation and boundary conditions of a continuously moving plate.

$$\frac{\partial U}{\partial X}+\frac{\partial V}{\partial Y}=0, \tag{1}$$

$$\frac{\partial}{\partial X}(U^2)+\frac{\partial}{\partial Y}(UV)-\frac{1}{Re_L}\left(\frac{\partial^2 U}{\partial X^2}+\frac{\partial^2 U}{\partial Y^2}\right)=-\frac{\partial P}{\partial X}, \tag{2}$$

$$\frac{\partial}{\partial X}(UV)+\frac{\partial}{\partial Y}(V^2)-\frac{1}{Re_L}\left(\frac{\partial^2 V}{\partial X^2}+\frac{\partial^2 V}{\partial Y^2}\right)=-\frac{\partial P}{\partial Y}, \tag{3}$$

$$\frac{\partial}{\partial X}(U\Theta)+\frac{\partial}{\partial Y}(V\Theta)-\frac{1}{Re_L Pr}\left(\frac{\partial^2 \Theta}{\partial X^2}+\frac{\partial^2 \Theta}{\partial Y^2}\right)=0. \tag{4}$$

The following scales $[L,\ u_w,\ (T_w-T_\infty),\ \rho u_w^2]$ are chosen for the length, velocity, temperature and pressure, respectively, to make the governing equations dimensionless. The above set of equations can be represented by a single equation of the form

$$\frac{\partial}{\partial X}(U\phi)+\frac{\partial}{\partial Y}(V\phi)-\frac{\Gamma_\phi}{Re_L}\left(\frac{\partial^2 \phi}{\partial X^2}+\frac{\partial^2 \phi}{\partial Y^2}\right)=S_\phi, \tag{5}$$

where ϕ is the general variable and stands for 1, U, V, and Θ in Eqs. (1)–(4), respectively; Γ_ϕ is the dimensionless exchange (diffusion) coefficient and stands for 0, 1, 1, and $1/Pr$ in the above equations, respectively; and S_ϕ is the source term and represents the right-hand side in the equations set for ϕ. This general form of transport equation facilitates the use of the same solution procedure to be applied to all governing equations.

2.2. Boundary conditions

With reference to Fig. 1, where the stretching plate is drawn horizontally through the slit at $x=0$, the following boundary conditions are applied. Starting with conditions at the surface ($y=0$):

$$u=u_w,\quad v=v_w(x)\quad\text{and}\quad T=T_w, \tag{6}$$

Table 1
Comparison of $Nu_x Re_x^{-0.5}$ in the self-similar region to previously published data for various d and Pr

d	Pr	Ali (1995)	Jacobi (1993)	Tsou et al. (1967)	Erickson et al. (1966)	Present study
0.0	0.7	0.3476	0.3492	0.3492	–	0.351
0.0	1.0	0.4416	0.4438	0.4438	0.4437	0.444
0.0	10.0	1.6713	1.679	1.6804	1.680	1.665
−0.25	1.0	–	–	–	0.604	0.607
−0.25	10.0	–	–	–	3.537	3.568
0.25	1.0	–	–	–	0.3097	0.310
0.25	10.0	–	–	–	0.4661	0.461

where u_w and T_w are constants. In order to allow for fluid injection or suction through the plate, the plate is regarded to be porous with a transpired velocity v_w given by

$$v_w = d\,u_w Re_x^{-1/2} \quad \text{or} \quad d = \frac{v_w}{u_w} Re_x^{1/2}, \tag{7}$$

where d is a suction/injection parameter. Such a velocity distribution is required to achieve similarity solutions far downstream from the slit (Ali, 1995). However, in the present numerical model, there is no restriction to such a specification since the practical situation may demand different distributions of velocities for the fluid injected or sucked through the stretching plate. Nevertheless, the distribution as given by Eq. (7) is retained to facilitate comparisons with solutions based on the similarity approach and to distinguish the nonsimilar from the similar regions in terms of Reynolds number. Positive or negative v_w implies injection or suction, respectively.

The left-hand side of the calculation domain, Fig. 1, simulates an impervious wall at which the following boundary conditions are applied:

$$u = 0, \quad v = 0 \quad \text{and} \quad T = T_\infty. \tag{8}$$

The top boundary is located far enough above the slit, therefore the following conditions are applied:

$$u = 0, \quad v = v_e, \quad T = T_\infty \quad \text{and} \quad p = p_\infty. \tag{9}$$

This boundary is allowed to entrain fluid at velocity v_e and temperature T_∞. The velocity v_e is not known beforehand and is determined iteratively by the calculations. Its value depends upon the mass flow rate drawn outside the calculation domain, by the drag force imposed by the moving plate on the adjacent fluid, and the mass flow rate being injected or sucked through the plate.

The following outlet conditions are applied at the right boundary of the calculation domain:

$$\frac{\partial u}{\partial x} = 0, \quad \frac{\partial v}{\partial x} = 0, \quad \frac{\partial T}{\partial x} = 0 \ \text{and} \ p = p_\infty. \tag{10}$$

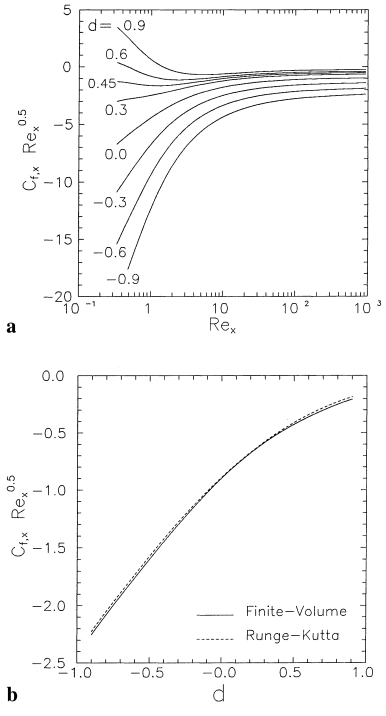

Fig. 2. Skin-friction coefficient variations with: (a) the Reynolds number for various suction/injection parameters d, and (b) the suction/injection parameter showing comparison between the finite-volume method and similarity method far downstream (large Reynolds number).

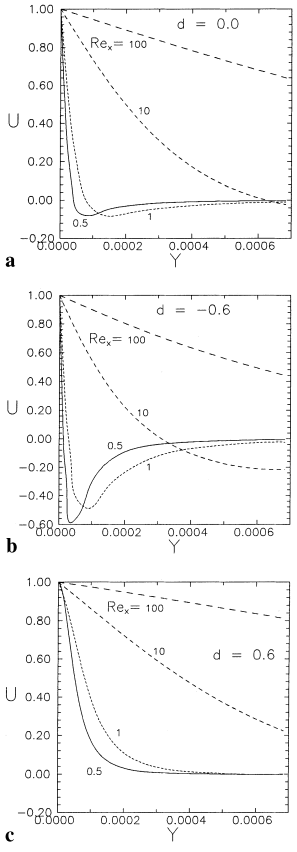

Fig. 3. Dimensionless velocity profiles for Reynolds numbers = 0.5 to 100 as a function of the transverse coordinate Y for different suction/injection parameters d: (a) $d = 0.0$, (b) $d = -0.6$, and (c) $d = 0.6$.

These approximate fully developed conditions and are quite adequate in the parabolic flow region especially when they are ensured to be located far downstream from the slit.

3. Numerical solution procedure

The numerical model uses a control-volume finite-difference method for discretizing the governing partial-differential equations (1)–(4). The pressure field and velocities are determined via the well-known SIMPLE algorithm of Patankar and Spalding (1972), but differs from it in the way the finite-volume equations are solved. The 2/E/FIX computer program of Pun and Spalding (1977) is modified and used to solve the present problem. The finite-volume equations are handled by this code on a line-by-line manner. Al-Sanea et al. (1980) and Al-Sanea (1992) have briefly described and applied the line-by-line procedure in computing recirculating flows with heat transfer. The scheme was found particularly beneficial for flows where relatively large parabolic or nearly parabolic regions exist alongside the elliptic flow regions. The present moving plate problem with suction or injection falls into such a category; elliptic effects are dominant very close to the slit region, whereas downstream of the slit the flow is predominantly parabolic.

All the numerical results are checked to be substantially grid independent. This is achieved by obtaining solutions with an increasing number of grid nodes until a stage is reached where the solution exhibits negligible change with further increase in the number of nodes. The top and outlet boundaries of the calculation domain are checked by numerical experiments to be located far enough not to influence the results in the region of interest. The location of the top boundary depends on Re, Pr and d; the lower the Re and Pr the higher its position should be, as, indeed, with increasing injection since it acts to thicken the boundary layer. For the range of parameters considered in the present study, the top boundary is located at a height of about 20% L which is greater than twice the maximum thickness of the boundary layers present at the very end of the plate.

A highly nonuniform finite-volume grid is used with nodes closely packed in regions with steep variation of flow properties; namely, very near to the extrusion slit and the moving plate. A typical grid size of 70×30 nodes in the x- and y-directions, respectively, is employed for all runs with $Pr \leqslant 3$. The grid step sizes, Δx and Δy, are both increasing in the x- and y-directions (see Fig. 1) with expansion factors of 1.15 and 1.5, respectively. Due to the much thinner thermal boundary layer for $Pr = 10$, the grid size in the y-direction is increased to 50 nodes with an expansion factor of 1.1 for injection and 1.3 for suction.

Converged solutions are achieved when the changes in all variables, for all nodes, produced by successive iterations diminish and when the sums of the normalized absolute values of residual errors in the finite-volume equations are reduced to a prescribed small value. Typical converged results are obtained after about 300 iterations starting from uniform initial-variable-field values; a near optimum relaxation factor of 0.7 is applied for all dependent variables. The calculations require

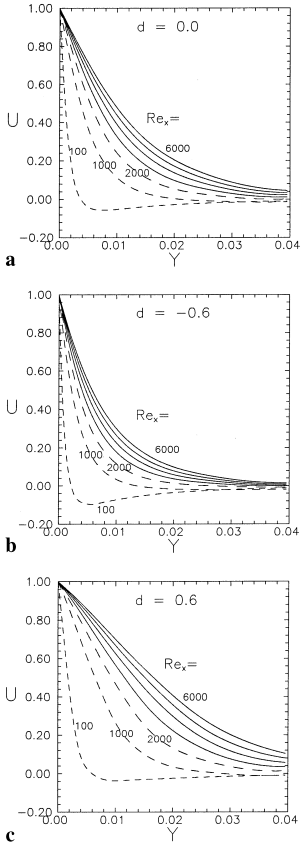

Fig. 4. Dimensionless velocity profiles for Reynolds numbers = 100 to 6000 as a function of the transverse coordinate Y for different suction/injection parameters d: (a) $d = 0.0$, (b) $d = -0.6$, and (c) $d = 0.6$.

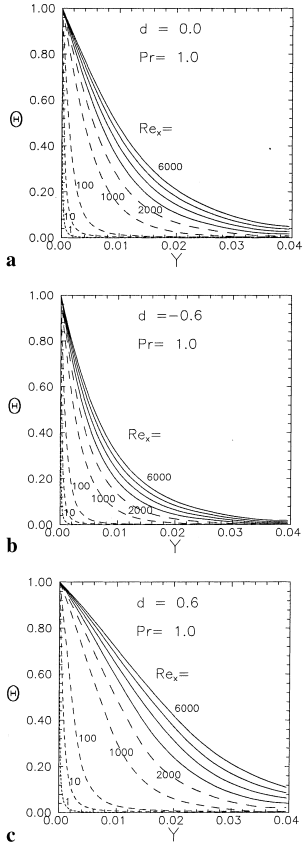

Fig. 5. Dimensionless temperature profiles for various Reynolds numbers as a function of the transverse coordinate Y for $Pr = 1$ and different suction/injection parameters d: (a) $d = 0.0$, (b) $d = -0.6$, and (c) $d = 0.6$.

about 1.3×10^{-5} s of CPU time per (iteration × variable × grid node) on a Pentium 200 MMX micro-computer.

4. Results and discussion

Results are presented for a continuously moving flat plate in an otherwise quiescent medium with Prandtl numbers of 0.1, 1, 3, and 10, and for different values of suction/injection parameter d. The plate is assumed to move with a uniform velocity and to be at a uniform temperature greater than the ambient temperature. The numerical model is validated by comparing results in the self-similar region with the similarity method solution and with results available in the literature. Table 1 gives $Nu_x Re_x^{-0.5}$ for various values of d and Pr; $d = 0$ for no suction or injection, is −ve for suction, and +ve for injection. The general agreement between the results is judged to be excellent.

The shear stress along the plate is presented in a dimensionless form of $C_{f,x} Re_x^{0.5}$ versus Re_x for various values of d in Fig. 2(a). For a fixed d, $C_{f,x} Re_x^{0.5}$ reaches asymptotically a constant value independent of Re_x far downstream from the slit, where the self-similar region exists. The initial variation of $C_{f,x} Re_x^{0.5}$ with Re_x is a distinguishing feature of the nonsimilar region close to the extrusion slit (low Re_x). This region is also characterized by much larger skin-friction coefficients which increase with increasing suction, or with increasing injection above $d \approx 0.45$. However, in the self-similar region injection acts only to reduce the friction coefficient. Furthermore, negative values of $C_{f,x} Re_x^{0.5}$ signify that the plate velocity is higher than the adjacent fluid velocity; the positive values indicate the opposite due to velocity overshoot caused by larger injection ($d \geqslant 0.45$). At $d \approx 0.45$, $C_{f,x} Re_x^{0.5}$ is almost constant and equal to the asymptotic value downstream; this value of injection parameter gives the lowest skin-friction coefficient in the region very close to the slit.

The Reynolds number required to achieve a local value of $C_{f,x} Re_x^{0.5}$ equals to 1.05 times the asymptotic value in the self-similar region, corresponding to each d, is defined as the critical Reynolds number $(Re_{x,c})_v$. This $(Re_{x,c})_v$ is used to distinguish the nonsimilar from the self-similar regions for the velocity boundary layer. The results show that $(Re_{x,c})_v$ is a weak function of d and that for $-0.9 \leqslant d \leqslant 0$, $(Re_{x,c})_v \approx 1000$; and for $0 < d \leqslant 0.9$, $(Re_{x,c})_v \approx 1150$. In other words, injection acts to delay arriving at the self-similar region. Therefore, the boundary layer approximations are valid in the region beyond $(Re_{x,c})_v$; whereas the full equations should be used for $Re_x < (Re_{x,c})_v$.

The asymptotic values of $C_{f,x} Re_x^{0.5}$ obtained by the finite-volume method are plotted versus d and compared with the results obtained by the similarity method using the fourth-order Runge–Kutta scheme in the self-similar region in Fig. 2(b). The comparison shows an excellent agreement and gives further validation to the current numerical model. The results also show that increasing suction acts to increase the skin-friction coefficient, while increasing injection does the opposite.

Samples of normalized velocity profiles are presented in Figs. 3(a)–(c) and 4(a)–(c) at different streamwise locations

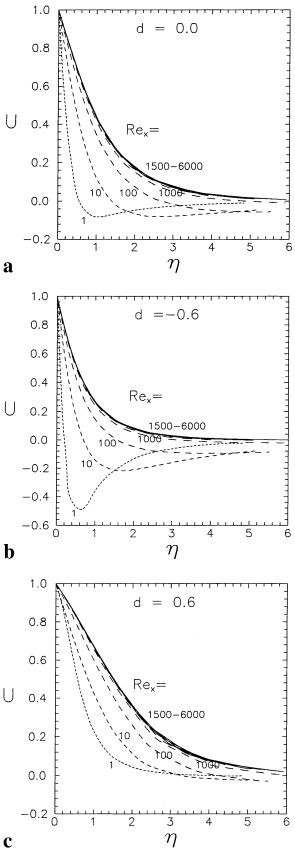

Fig. 6. Dimensionless velocity profiles for various Reynolds numbers as a function of the similarity variable η for different suction/injection parameters d: (a) $d = 0.0$, (b) $d = -0.6$, and (c) $d = 0.6$.

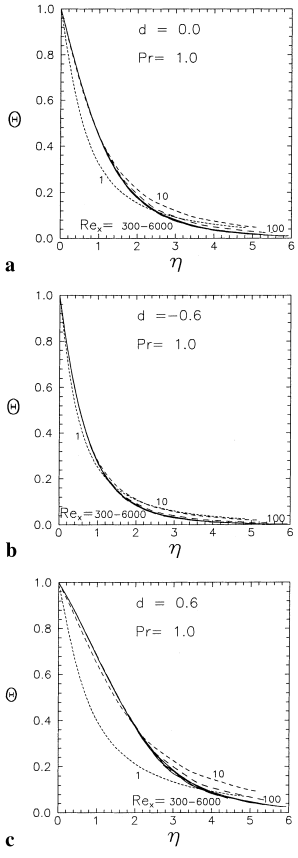

Fig. 7. Dimensionless temperature profiles for various Reynolds numbers as a function of the similarity variable η for $Pr = 1$ and different suction/injection parameters d: (a) $d = 0.0$, (b) $d = -0.6$, and (c) $d = 0.6$.

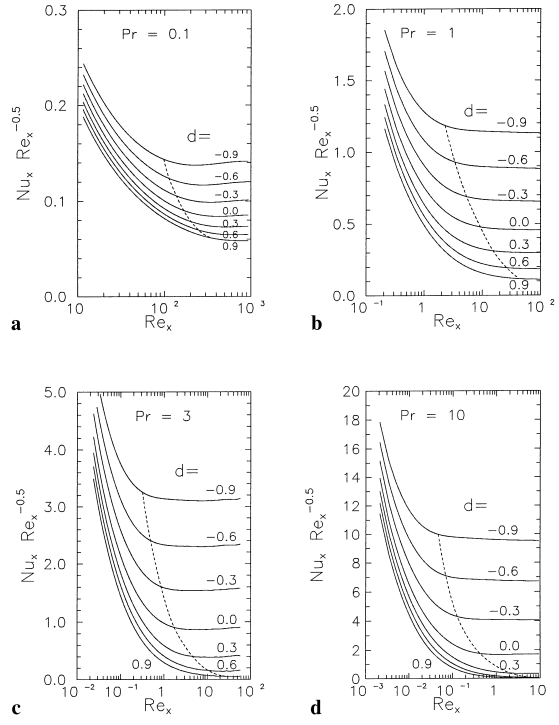

Fig. 8. Nusselt number distributions for different suction/injection parameters d as a function of Reynolds number for: (a) $Pr = 0.1$, (b) $Pr = 1$, (c) $Pr = 3$, and (d) $Pr = 10$; nonsimilar regions exist to the left of dashed lines with the self-similar regions to the right.

given by Re_x and for different d. Figs. 3(a)–(c) show the effect of increasing Re_x from 0.5 to 100, very close to the slit, on the velocity profiles for no suction or injection $d = 0.0$ in Fig. 3(a), for suction with $d = -0.6$ in Fig. 3(b), and in Fig. 3(c) for injection with $d = 0.6$. Figs. 4(a)–(c) give, respectively, the corresponding results for Re_x up to 6000, far downstream from the slit. It is clear that close to the slit where $Re_x < 1000$, there exists a region of reverse flow (−ve U) and hence the flow is directed opposite to the direction of the moving plate. This reverse flow is a consequence of the large pressure gradient directed toward the slit at $X = Y = 0$ due to the motion of the plate. However, this effect is found to decay downstream for $Re_x > 1000$. It is clear that suction acts to increase the size of the reverse flow region, whereas injection reduces it. It is also noted that the streamwise velocity reaches asymptotically the stagnant ambient value ($U = 0$) as Y increases. The thickness of the velocity boundary layer increases with increasing Re_x and injection and decreases with increasing suction.

Figs. 5(a)–(c) show the corresponding dimensionless temperature profiles for $Pr = 1$. It is clear that suction reduces the thermal boundary layer thickness whereas injection thickens it. Furthermore, as Re_x decreases the temperature gradient at the surface gets steeper which indicates that a higher heat flux is transferred to the medium near the slit than downstream at high Re_x. It may be noted that for $Re_x < 1500$, the thermal boundary layer thickness is greater than that of the velocity due to the existence of reverse flow outside the boundary layer region.

Figs. 6(a)–(c) are constructed using the similarity variable η. As shown, the velocity profiles for $Re_x \geqslant 1500$ collapse on one curve; these distinguish the self-similar region where the boundary layer approximations are valid. In the region where $(Re_{x,c})_v \leqslant Re_x < 1500$, the slopes of the velocity profiles are identical only close to the surface. Near the slit, $Re_x < (Re_{x,c})_v$, it is clear that the velocity profiles are different and nonsimilar. This distinguishes the nonsimilar region in which the boundary layer approximations break down. The temperature profiles as a function of η are presented in Figs. 7(a)–(c) for the same parameters as in Figs. 6(a)–(c) and for $Pr = 1$. As shown, the temperature profiles for $Re_x \geqslant 300$ are similar and collapse on one curve throughout the thermal boundary layer. Corresponding temperature profiles are obtained for $Pr = 0.1,\ 3,\ 10$ and are not presented here to conserve space.

The local heat-transfer coefficient variations with Reynolds number for different d and for $Pr = 0.1,\ 1,\ 3$ and 10 are shown in Figs. 8(a)–(d), respectively, in terms of $Nu_x Re_x^{-0.5}$. It is clear from these figures that the heat-transfer coefficient increases with suction and decreases with injection. Besides, this effect is greater for larger Pr since the temperature boundary layer is thinner and hence the temperature gradients at the surface are steeper. Moreover, the increase in heat-transfer coefficient is significant as Re_x decreases for a given d where the temperature gradients get steeper still toward the slit.

With increasing Re_x, the product $Nu_x Re_x^{-0.5}$ attains asymptotically a constant value independent of Re_x in the self-similar region; this asymptotic value depends on both d and Pr. At smaller Re_x, $Nu_x Re_x^{-0.5}$ becomes Re_x dependent too and increases sharply toward the slit. This behavior is used to distinguish the self-similar from the nonsimilar regions. Based on a similar definition used for the hydrodynamics, critical Reynolds numbers are calculated at which the products $Nu_x Re_x^{-0.5}$ attain local values equal to 1.05 times the asymptotic values in the self-similar region. Table 2 lists these critical Reynolds numbers $(Re_{x,c})_T$ and the corresponding values of $Nu_x Re_x^{-0.5}$ for each d and Pr. Furthermore, in Figs. 8(a)–(d) dashed lines are plotted to connect these points and, hence, separate the self-similar from the nonsimilar regions. Therefore, the boundary layer approximations are valid in the regions to the right of the dashed lines and break down in the regions to the left. The results show that for higher Prandtl number fluids, $(Re_{x,c})_T$ gets smaller. The value of $(Re_{x,c})_T$ is of the order 1 for $Pr = 3$ to 10

Table 2
Critical Reynolds numbers and corresponding $Nu_x Re_x^{-0.5}$ at which the dimensionless temperature gradients at the surface become equal for various d and Pr

d	$Pr = 0.1$		$Pr = 1.0$		$Pr = 3.0$		$Pr = 10.0$	
	$(Re_{x,c})_T$	$Nu_x Re_x^{-0.5}$	$(Re_{x,c})_T$	$Nu_x Re_x^{-0.5}$	$(Re_{x,c})_T$	$Nu_x Re_x^{-0.5}$	$(Re_{x,c})_T$	$Nu_x Re_x^{-0.5}$
−0.9	99	0.143	2.3	1.183	0.32	3.256	0.05	9.992
−0.6	114	0.124	3.4	0.923	0.49	2.409	0.07	7.031
−0.3	140	0.104	5.4	0.684	0.86	1.609	0.13	4.237
0.0	173	0.088	9.3	0.473	1.73	0.908	0.42	1.750
0.3	210	0.077	15.3	0.310	4.61	0.404	2.10	0.358
0.6	264	0.067	25.7	0.195	11.00	0.148	9.00	0.046
0.9	349	0.061	42.0	0.118	28.42	0.051	19.00	0.005

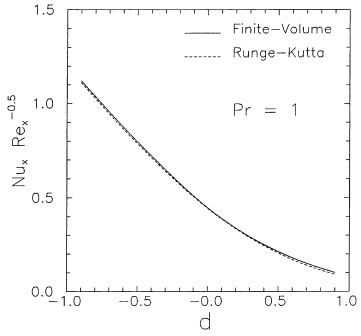

Fig. 9. Nusselt number variation with the suction/injection parameter for $Pr = 1$ showing comparison between the finite-volume method and similarity method far downstream (large Reynolds number).

(water and similar liquids) and is of the order 100 to 10 for $Pr = 0.1$ to 1 (gases in general); suction acts to decrease $(Re_{x,c})_T$, whereas injection acts to increase it. Referring back to Figs. 7(a)–(c) and for $Re_x > (Re_{x,c})_T$, it is noted that the slopes of the temperature profiles at the surface are the same. Therefore, $(Re_{x,c})_T$ is used to distinguish between the self-similar and nonsimilar regions as given in Table 2.

The asymptotic values of $Nu_x Re_x^{-0.5}$ obtained by the finite-volume method are plotted versus d and compared with the similarity method results using the fourth-order Runge–Kutta scheme in the self-similar region in Fig. 9. The comparison shows an excellent agreement which further demonstrates the accuracy and validity of the numerical model. The results also indicate an order of magnitude increase in the value of Nusselt number due to suction at $d = -0.9$ as compared to injection at $d = 0.9$.

The dimensionless pressure contours are presented in Figs. 10(a)–(c) for $d = 0$, -0.6 and 0.6, respectively. The pressure values are normalized by ρu_w^2, and the region only very close to the slit is shown; outside this region, the pressure is practically uniform. The contour interval is fixed constant at 0.02. It is clearly seen that the pressure gradient increases sharply toward the corner, where the slit is, due to the motion of the plate and the presence of the stagnant left wall above the slit. This is why the reverse flow exists in this region as seen in the velocity profiles in Figs. 3, 4 and 6. The pressure level and gradients increase as suction is introduced at the surface and decrease with injection.

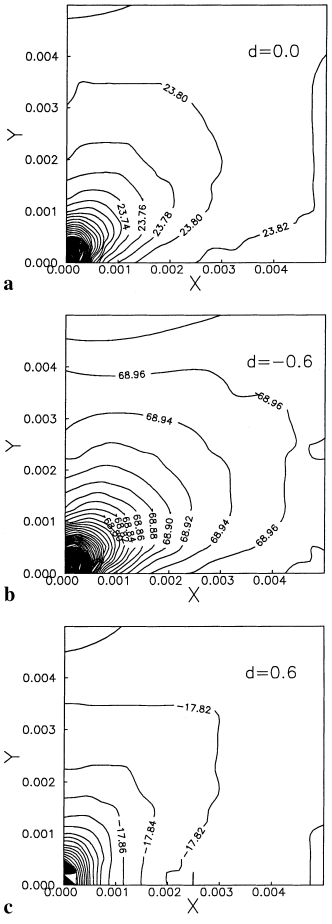

Fig. 10. Pressure contours over a stretched surface for different suction/injection parameters d: (a) $d = 0.0$, (b) $d = -0.6$, and (c) $d = 0.6$.

5. Conclusions

The finite-volume method is used to solve the full equations of motion due to a moving surface in a quiescent medium with suction or injection at the surface. The surface is assumed to move at a uniform speed with a uniform temperature in four Prandtl number fluids of 0.1, 1, 3, and 10.

For the range of parameters studied, the results show that the velocity profiles for $Re_x < 1000$ have reverse flow regions, and for $Re_x < 1500$ the profiles are nonsimilar. Critical Reynolds numbers $(Re_{x,c})_v$, based on asymptotic values of friction coefficients, are calculated at about 1000 for suction and 1150 for injection. For $(Re_{x,c})_v < Re_x < 1500$, the velocity profiles versus η have the same slope only close to the surface. For $Re_x > 1500$, the whole profiles become similar and collapse on one curve. The same trend is obtained for the thermal characteristics which show dependency on Pr too. Critical Reynolds numbers, $(Re_{x,c})_T$, are obtained to distinguish the nonsimilar from the similar regions, with d and Pr as parameters, as given in Table 2. Furthermore, rapid increase in heat-transfer coefficient is calculated with decreasing Re_x; the heat-transfer coefficient increases with Pr and suction and decreases with injection. On the other hand, $Nu_x Re_x^{-0.5}$ reaches asymptotic values, with increasing Re_x, equal to those obtained by the similarity method with magnitudes depending on d and Pr.

Finally, the skin-friction coefficients attain large values at low Re_x. The product $C_{f,x} Re_x^{0.5}$ reaches asymptotically, with increasing Re_x, a constant value obtained by the similarity method for a particular d. In the self-similar region, the skin-friction coefficient increases with suction and decreases with injection as long as the boundary layer does not separate. In the nonsimilar region, the behavior of the friction coefficient is slightly more complicated since it depends on Re_x too, and increasing injection above $d \approx 0.45$ can lead to an increase in the friction coefficient, due to velocity overshoot, close to the slit.

References

Ali, M.E., 1994. Heat transfer characteristics of a continuous stretching surface. Wärme- und Stoffübertragung 29, 227–234.

Ali, M.E., 1995. On thermal boundary layer on a power-law stretched surface with suction or injection. Int. J. Heat Fluid Flow 16 (4), 280–290.

Ali, M.E., Al-Yousef, F., 1997. Heat transfer and flow field on an extruded vertical material. In: Proceedings of the 10th Interna-

tional Conference of Mech. Power Engineering, Assiut University, Assiut, Egypt,16–18 December, pp. 207–219.

Ali, M.E., Al-Yousef, F., 1998. Laminar mixed convection from a continuously moving vertical surface with suction or injection. Heat Mass Transfer 33 (4), 301–306.

Al-Sanea, S.A., 1992. A numerical study of the flow and heat-transfer characteristics of an impinging laminar slot-jet including crossflow effects. Int. J. Heat Mass Transfer 35 (10), 2501–2513.

Al-Sanea, S.A., Pun, W.M., Spalding, D.B., 1980. Computation of two-dimensional elliptic flows, including heat transfer. In: Morgan, K., Taylor, C., Brebbia, C.A. (Eds.), Computer Methods in Fluids. Pentech Press, London, pp. 217–256.

Altan, T., Oh, S., Gegel, H., 1979. Metal Forming Fundamentals and Applications. American Society of Metals, Metals Park, OH.

Chen, C.K., Char, M.I., 1988. Heat transfer of a continuous stretching surface with suction or blowing. J. Math. Anal. Appl. 135, 568–580.

Crane, L.J., 1970. Flow past a stretching plane. Z. Amgew. Math. Phys. 21, 645–647.

Erickson, L.E., Fan, L.T., Fox, V.G., 1966. Heat and mass transfer on a moving continuous flat plate with suction or injection. Ind. Eng. Chem. Fundam. 5, 19–25.

Fisher, E.G., 1976. Extrusion of Plastics. Wiley, New York.

Fox, V.G., Erickson, L.E., Fan, L.T., 1968. Methods for solving the boundary layer equations for moving continuous flat surfaces with suction and injection. AIChE J. 14, 726–736.

Grubka, L.G., Bobba, K.M., 1985. Heat transfer characteristics of a continuous stretching surface with variable temperature. ASME J. Heat Transfer 107, 248–250.

Gupta, P.S., Gupta, A.S., 1977. Heat and mass transfer on a stretching sheet with suction or blowing. Canad. J. Chem. Eng. 55 (6), 744–746.

Jacobi, A.M., 1993. A scale analysis approach to the correlation of continuous moving sheet (backward boundary layer) forced convective heat transfer. ASME J. Heat Transfer 115, 1058–1061.

Kang, B.H., Jaluria, Y., 1993. Thermal modeling of the continuous casting process. J. Thermophysics Heat Transfer 7 (1), 139–147.

Karwe, M.V., Jaluria, Y., 1988. Fluid flow and mixed convection transport from a moving plate in rolling and extrusion processes. ASME J. Heat Transfer 110, 655–661.

Karwe, M.V., Jaluria, Y., 1991. Numerical simulation of thermal transport associated with a continuously moving flat sheet in materials processing. ASME J. Heat Transfer 113, 612–619.

Lakshmisha, K.N., Venkateswaran, S., Nath, G., 1988. Three dimensional unsteady flow with heat and mass transfer over a continuous stretching surface. ASME J. Heat Transfer 110, 590–595.

Patankar, S.V., Spalding, D.B., 1972. A calculation procedure for heat, mass and momentum transfer in three-dimensional parabolic flows. Int. J. Heat Mass Transfer 15, 1787–1806.

Pun, W.M., Spalding, D.B., 1977. A general computer program for two dimensional elliptic flows. Report No. HTS/76/2, Department of Mechanical Engineering, Imperial College, London.

Sakiadis, B.C., 1961. Boundary layer behavior on continuous solid surfaces: I. boundary-layer equations for two-dimensional and axisymmetric flow. AIChE J. 7 (1), 26–28.

Soundalgekar, V.M., Ramana Murty, T.V., 1980. Heat transfer past a continuous moving plate with variable temperature. Wärme- und Stoffübertragung 14, 91–93.

Tadmor, Z., Klein, I., 1970. Engineering Principles of Plasticating Extrusion, Polymer Science and Engineering Series. Van Nostrand Reinhold, New York.

Tsou, F.K., Sparrow, E.M., Goldstein, R.J., 1967. Flow and heat transfer in the boundary layer on a continuous moving surface. Int. J. Heat Mass Transfer 10, 219–235.